Lorentz-Augmented Spacecraft Formation Reconfiguration

Ludwik A. Sobiesiak and Christopher J. Damaren

***Abstract*— The use of the geomagnetic Lorentz force as a means of actuation is considered in this paper for the purpose of spacecraft formation reconfiguration. A continuous/impulsive linear quadratic regulator (LQR) is proposed for the purpose of designing an optimal control strategy that combines continuous Lorentz force actuation with impulsive thrusting. New theory is presented for the determination of optimal impulsive thrust application time. A simulation of a spacecraft formation reconfiguration maneuver demonstrates the effectiveness of the continuous/impulsive LQR.**

***Index Terms*— Hybrid continuous/impulsive optimal control, Lorentz-augmented formation flight, spacecraft formation flying.**

I. Introduction

THIS paper explores performing spacecraft formation reconfiguration with the aid of the geomagnetic Lorentz force. The Lorentz force is the force experienced by a charged particle as it moves through a magnetic field. In the context of this paper, the particle is a charge-carrying spacecraft and the magnetic field is the earth's magnetic field. Peck [1] first proposed the use of the geomagnetic Lorentz force as a means of actuation for spacecraft. In low earth orbit, the relative velocity of the spacecraft with respect to the geomagnetic field is large enough that a modest charge on the spacecraft can result in a meaningful acceleration. Through the modulation of such a charge, a means of propellantless propulsion can be achieved.

References [2]–[5] that explore Lorentz-augmented formation flight focus exclusively on using relative Cartesian coordinates to model the spacecraft relative motion. This paper uses mean differential orbital elements as the plant model of the relative spacecraft dynamics for controller design. A key aspect of this approach is the use of Gauss's variational equations to establish a linear time-varying (LTV) model [6]. Sobiesiak and Damaren [7]–[9] have explored the use of the Lorentz force for the purpose of spacecraft formation-keeping in the presence of disturbances such as the J_2 zonal harmonic, caused by the earth's oblateness. Due to the constrained nature of the Lorentz force, it was identified that the deputy spacecraft state relative to the chief spacecraft is not entirely controllable by use of the Lorentz force alone [9]. Some supplemental thrust control effort must be used to drive an initial relative state to a desired final state.

The objective of this research is to combine the continuously acting Lorentz force control effort with the minimal amount of thruster control effort needed to control the formation. This goal led to the development of the hybrid continuous/impulsive linear quadratic regulator (LQR) presented in [8], which built upon the theory in [10] and [11]. The theory, however, was limited to prescribed impulse application times. In this paper, the hybrid LQR theory is extended so that a performance index, J, is minimized not only with respect to continuous and impulsive control inputs but also with respect to the time at which the impulsive action is applied. A preliminary version of the theory was presented in [12].

This new theory is applied to the Lorentz-augmented spacecraft formation reconfiguration problem. The relative spacecraft state is described using mean differential orbital elements, whose dynamics include the secular effects of the J_2 perturbation. A preliminary version of this paper was presented in [13]. Other approaches to spacecraft formation establishment and reconfiguration using impulsive thruster inputs exclusively can be found in [14]–[16]. It is noteworthy that [15] optimized the timing of the impulsive inputs.

Use of the Lorentz force in the fashion described here is currently at a low state of technology readiness. This paper explores a possible application of the Lorentz force, but determining how a spacecraft would generate and store the charge necessary to employ the Lorentz force is beyond the scope of this paper.

II. Control of Systems With Continuous and Impulsive Inputs

The following state-space representation of a continuous/impulsive LTV system is considered, with $N-1$ impulsive actions being applied at $t = t_k$, $k = 1, \ldots, N-1$

$$\dot{\mathbf{x}} = \mathbf{A}(t)\mathbf{x}(t) + \mathbf{B}(t)\mathbf{u}(t), \quad t \neq t_k \tag{1}$$

$$\mathbf{x}(t_k^+) = \mathbf{C}_k\mathbf{x}(t_k^-) + \mathbf{D}_k\mathbf{v}_k, \quad t = t_k \tag{2}$$

where $\mathbf{x}(t) \in \mathbb{R}^n$ is the state, $\mathbf{u}(t) \in \mathcal{U}$, a bounded set of admissible controls in $\mathbb{R}^m$, is the piecewise continuous control, and $\mathbf{v}_k \in \mathcal{V}$, a bounded set of admissible impulsive controls in $\mathbb{R}^l$, is the impulsive control. The superscripts $(\cdot)^-$ and $(\cdot)^+$ denote the instant immediately before and after the impulsive dynamics are applied, respectively. In the problem being considered, it is assumed that the number of impulses, $N-1$,

Manuscript received November 24, 2014; revised April 27, 2015; accepted July 18, 2015. Manuscript received in final form July 23, 2015. Recommended by Associate Editor Q. Wang.

The authors are with the Institute for Aerospace Studies, University of Toronto, Toronto, ON M3H 5T6, Canada (e-mail: l.sobiesiak@gmail.com; damaren@utias.utoronto.ca).

Color versions of one or more of the figures in this paper are available online at http://ieeexplore.ieee.org.

Digital Object Identifier 10.1109/TCST.2015.2461593

is prescribed but the times at which they are applied will be optimized. In particular, we seek controls $\mathbf{u}$ and $\mathbf{v}_k$, along with times t_k, $k = 1, \ldots, N-1$, that minimize

$$\begin{aligned} J = &\frac{1}{2}\mathbf{x}^{\mathsf{T}}(t_f)\mathbf{K}\mathbf{x}(t_f) \\ &+ \frac{1}{2}\int_{t_0}^{t_f}[\mathbf{x}^{\mathsf{T}}(t)\mathbf{Q}(t)\mathbf{x}(t) + \mathbf{u}^{\mathsf{T}}(t)\mathbf{R}(t)\mathbf{u}(t)]dt \\ &+ \frac{1}{2}\sum_{k=1}^{N-1}\left[\mathbf{x}^{\mathsf{T}}\big(t_k^-\big)\mathbf{Q}_k\mathbf{x}\big(t_k^-\big) + \frac{1}{2}\mathbf{v}_k^{\mathsf{T}}\mathbf{R}_k\mathbf{v}_k\right] \end{aligned} \tag{3}$$

where $\mathbf{K} = \mathbf{K}^{\mathsf{T}} \geq \mathbf{0}$, $\mathbf{Q}(t) = \mathbf{Q}^{\mathsf{T}}(t) \geq \mathbf{0}$, $\mathbf{Q}_k = \mathbf{Q}_k^{\mathsf{T}} \geq \mathbf{0}$, $\mathbf{R}(t) = \mathbf{R}^{\mathsf{T}}(t) > \mathbf{0}$, and $\mathbf{R}_k = \mathbf{R}_k^{\mathsf{T}} > \mathbf{0}$. It is assumed that $\mathbf{x}(0)$ is prescribed.

The continuous and impulsive Hamiltonian functions are introduced as

$$\begin{aligned} \mathcal{H}_c = &\frac{1}{2}\mathbf{x}^{\mathsf{T}}(t)\mathbf{Q}(t)\mathbf{x}(t) + \frac{1}{2}\mathbf{u}^{\mathsf{T}}(t)\mathbf{R}(t)\mathbf{u}(t) \\ &+ \boldsymbol{\lambda}^{\mathsf{T}}(t)[\mathbf{A}(t)\mathbf{x}(t) + \mathbf{B}(t)\mathbf{u}(t)] \end{aligned} \tag{4}$$

$$\begin{aligned} \mathcal{H}_{d,k} = &\frac{1}{2}\mathbf{x}^{\mathsf{T}}\big(t_k^-\big)\mathbf{Q}_k\mathbf{x}\big(t_k^-\big) + \frac{1}{2}\mathbf{v}_k^{\mathsf{T}}\mathbf{R}_k\mathbf{v}_k \\ &+ \boldsymbol{\nu}_k^{\mathsf{T}}\big[\mathbf{C}_k\mathbf{x}\big(t_k^-\big) + \mathbf{D}_k\mathbf{v}_k\big]. \end{aligned} \tag{5}$$

The vectors $\boldsymbol{\lambda}(t)$ and $\boldsymbol{\nu}_k$ are two sets of costates that adjoin the continuous and impulsive dynamics, respectively. Using the Hamiltonian functions, the hybrid, quadratic cost functional becomes

$$\begin{aligned} J = &\frac{1}{2}\mathbf{x}^{\mathsf{T}}(t_f)\mathbf{K}\mathbf{x}(t_f) + \sum_{k=1}^{N-1}\big[\mathcal{H}_{d,k} - \boldsymbol{\nu}_k^{\mathsf{T}}\mathbf{x}\big(t_k^+\big)\big] \\ &+ \sum_{k=0}^{N-1}\int_{t_k^+}^{t_{k+1}^-}[\mathcal{H}_c - \boldsymbol{\lambda}^{\mathsf{T}}(t)\dot{\mathbf{x}}(t)]dt \end{aligned} \tag{6}$$

where $t_0^+ = t_0$ and $t_N^- = t_f$.

A. Necessary Conditions for Optimality

Variational principles are now applied to obtain necessary conditions for an extremum of the cost functional in (6). An extremum is sought not only with respect to the controls and states but also with respect to application time of the impulsive dynamics. To vary impulse application time, the noncontemporaneous variations or differentials of the state and control must be considered [17], e.g., the differential of the state vector must include the variation in application time

$$d\mathbf{x}\big(t_k^\pm\big) = \delta\mathbf{x}\big(t_k^\pm\big) + \dot{\mathbf{x}}\big(t_k^\pm\big)dt_k. \tag{7}$$

Taking the first differential of the cost functional yields

$$\begin{aligned} dJ = &\mathbf{x}^{\mathsf{T}}(t_f)\mathbf{K}d\mathbf{x}(t_f) \\ &+ \sum_{k=1}^{N-1}\left[\frac{\partial\mathcal{H}_{d,k}}{\partial\mathbf{x}\big(t_k^-\big)}^{\mathsf{T}}d\mathbf{x}\big(t_k^-\big) + \frac{\partial\mathcal{H}_{d,k}}{\partial\mathbf{v}_k}^{\mathsf{T}}d\mathbf{v}_k + \frac{\partial\mathcal{H}_{d,k}}{\partial t_k}dt_k\right. \\ &\left. - \boldsymbol{\nu}_k^{\mathsf{T}}d\mathbf{x}\big(t_k^+\big) + \frac{d}{dt_k}\sum_{l=0}^{N-1}\int_{t_l^+}^{t_{l+1}^-}(\mathcal{H}_c - \boldsymbol{\lambda}^{\mathsf{T}}\dot{\mathbf{x}})dt\,dt_k\right] \\ &+ \sum_{k=0}^{N-1}\int_{t_k^+}^{t_{k+1}^-}\left(\frac{\partial\mathcal{H}_c}{\partial\mathbf{x}}^{\mathsf{T}}\delta\mathbf{x}(t) + \frac{\partial\mathcal{H}_c}{\partial\mathbf{u}}^{\mathsf{T}}\delta\mathbf{u}(t) - \boldsymbol{\lambda}^{\mathsf{T}}(t)\delta\dot{\mathbf{x}}(t)\right)dt. \end{aligned} \tag{8}$$

Using Leibniz's rule of integration, the derivative of the integral terms with respect to t_k can be evaluated

$$\begin{aligned} &\sum_{k=1}^{N-1}\frac{d}{dt_k}\left[\sum_{l=0}^{N-1}\int_{t_l^+}^{t_{l+1}^-}(\mathcal{H}_c - \boldsymbol{\lambda}^{\mathsf{T}}\dot{\mathbf{x}})dt\right]dt_k \\ &\quad = \sum_{k=1}^{N-1}(\mathcal{H}_c - \boldsymbol{\lambda}^{\mathsf{T}}\dot{\mathbf{x}})|_{t_k^-}dt_k - (\mathcal{H}_c - \boldsymbol{\lambda}^{\mathsf{T}}\dot{\mathbf{x}})|_{t_k^+}dt_k. \end{aligned} \tag{9}$$

The terms containing $\dot{\mathbf{x}}(t_k^\pm)dt_k^\pm$ on the right-hand side of (9) can be combined with the result of integrating by parts the last term in (8). Doing this while using (7), we have

$$\begin{aligned} &-\sum_{k=0}^{N-1}\left[(\boldsymbol{\lambda}^{\mathsf{T}}(t)\dot{\mathbf{x}}(t)dt)|_{t_k^+}^{t_{k+1}^-} + \boldsymbol{\lambda}^{\mathsf{T}}(t)\delta\mathbf{x}(t)|_{t_k^+}^{t_{k+1}^-}\right] \\ &\quad = \sum_{k=1}^{N-1}\Big(\boldsymbol{\lambda}^{\mathsf{T}}\big(t_k^+\big)d\mathbf{x}\big(t_k^+\big) - \boldsymbol{\lambda}^{\mathsf{T}}\big(t_k^-\big)d\mathbf{x}\big(t_k^-\big)\Big) - \boldsymbol{\lambda}^{\mathsf{T}}(t_f)d\mathbf{x}(t_f) \end{aligned} \tag{10}$$

where it has been assumed that $\delta\mathbf{x}(0) = \mathbf{0}$, $t_N^- = t_f$, and $dt_0 = dt_N = 0$. Introducing this result and the terms containing $\mathcal{H}_c$ from (9) into (8) and collecting like terms yields

$$\begin{aligned} dJ = &\Big(\mathbf{x}^{\mathsf{T}}(t_f)\mathbf{K} - \boldsymbol{\lambda}^{\mathsf{T}}(t_f)\Big)\,d\mathbf{x}(t_f) \\ &+ \sum_{k=1}^{N-1}\left[\left(\mathcal{H}_c\big(t_k^-\big) - \mathcal{H}_c\big(t_k^+\big) + \frac{\partial\mathcal{H}_{d,k}}{\partial t_k}\right)dt_k\right. \\ &\quad + \big(\boldsymbol{\lambda}^{\mathsf{T}}\big(t_k^+\big) - \boldsymbol{\nu}_k^{\mathsf{T}}\big)d\mathbf{x}\big(t_k^+\big) + \frac{\partial\mathcal{H}_{d,k}}{\partial\mathbf{v}_k}^{\mathsf{T}}d\mathbf{v}_k \\ &\quad \left. + \left(\frac{\partial\mathcal{H}_{d,k}}{\partial\mathbf{x}\big(t_k^-\big)}^{\mathsf{T}} - \boldsymbol{\lambda}^{\mathsf{T}}\big(t_k^-\big)\right)d\mathbf{x}\big(t_k^-\big)\right] \\ &+ \sum_{k=0}^{N-1}\int_{t_k^+}^{t_{k+1}^-}\left[\left(\frac{\partial\mathcal{H}_c}{\partial\mathbf{x}}^{\mathsf{T}} + \dot{\boldsymbol{\lambda}}^{\mathsf{T}}(t)\right)\delta\mathbf{x}(t) + \frac{\partial\mathcal{H}_c}{\partial\mathbf{u}}^{\mathsf{T}}\delta\mathbf{u}(t)\right]dt. \end{aligned} \tag{11}$$

At an extremum of J, $dJ = 0$. Therefore, the continuous and impulsive costates are chosen such that

$$-\dot{\boldsymbol{\lambda}}(t) = \frac{\partial\mathcal{H}_c}{\partial\mathbf{x}} = \mathbf{Q}(t)\mathbf{x}(t) + \mathbf{A}^{\mathsf{T}}(t)\boldsymbol{\lambda}(t) \tag{12}$$

$$\boldsymbol{\lambda}\big(t_k^-\big) = \frac{\partial\mathcal{H}_{d,k}}{\partial\mathbf{x}\big(t_k^-\big)} = \mathbf{Q}_k\mathbf{x}(t_k^-) + \mathbf{C}_k^{\mathsf{T}}\boldsymbol{\nu}_k \tag{13}$$

$$\boldsymbol{\lambda}(t_f) = \mathbf{K}\mathbf{x}(t_f) \tag{14}$$

$$\boldsymbol{\nu}_k = \boldsymbol{\lambda}\big(t_k^+\big). \tag{15}$$

Note, the continuous and impulsive costates are related via the transversality condition in (15). The impulse application times, t_k, are chosen to satisfy the transversality condition

$$\Delta_k \equiv \mathcal{H}_c\big(t_k^-\big) - \mathcal{H}_c\big(t_k^+\big) + \frac{\partial\mathcal{H}_{d,k}}{\partial t_k} = 0 \tag{16}$$

for $k = 1, \ldots, N-1$. Finally

$$\frac{\partial\mathcal{H}_c}{\partial\mathbf{u}} = \mathbf{0} \tag{17}$$

$$\frac{\partial\mathcal{H}_{d,k}}{\partial\mathbf{v}_k} = \mathbf{0} \tag{18}$$

can be used to determine the optimal controls; however, a controllability argument must be made to justify (17) and (18), since $\delta\mathbf{u}(t)$ and $d\mathbf{v}_k$ are not completely arbitrary [17]. Together, (12)–(18) are the necessary conditions for determining an extremum of J.

B. Optimal Controls

From (17) and (18), the optimal continuous and impulsive control inputs are

$$\mathbf{u}^*(t) = -\mathbf{R}^{-1}(t)\mathbf{B}^{\mathsf{T}}(t)\boldsymbol{\lambda}(t) \tag{19}$$

$$\mathbf{v}_k^* = -\mathbf{R}_k^{-1}\mathbf{D}_k^{\mathsf{T}}\boldsymbol{\nu}_k \tag{20}$$

where $(\cdot)^*$ denotes the optimal quantity. Taking (1), with (19) substituted for $\mathbf{u}(t)$, together with (12) forms the continuous regulator two-point boundary value problem for which the linear relationship

$$\boldsymbol{\lambda}(t) = \mathbf{P}(t)\mathbf{x}(t) \tag{21}$$

with $\mathbf{P}(t_f) = \mathbf{K}$ is well known [18]. Taking the temporal derivative of (21) and substituting in (1) and (12) with (19) and (21) yields the well-known continuous matrix Riccati equation

$$\begin{aligned}-\dot{\mathbf{P}}(t) = {}& \mathbf{Q}(t) + \mathbf{A}^{\mathsf{T}}(t)\mathbf{P}(t) + \mathbf{P}(t)\mathbf{A}(t) \\ & -\mathbf{P}(t)\mathbf{B}(t)\mathbf{R}^{-1}(t)\mathbf{B}^{\mathsf{T}}(t)\mathbf{P}(t)\end{aligned} \tag{22}$$

and in the context of the continuous/impulsive control problem is valid for each time interval $t \in [t_k^+, t_{k+1}^-]$. In the sequel, we will need a boundary condition for $\mathbf{P}(t_{k+1}^-)$ (with $\mathbf{P}(t_N^-) = \mathbf{K}$) from which (22) can be integrated backward.

For the impulsive control, a similar development follows. Substituting (20) into (2) and substituting (15) for $\boldsymbol{\nu}_k$ into (13) yields a system that is analogous to the well-known discrete-time regulator two-point boundary value problem

$$\mathbf{x}(t_k^+) = \mathbf{C}_k\mathbf{x}(t_k^-) - \mathbf{D}_k\mathbf{R}_k^{-1}\mathbf{D}_k^{\mathsf{T}}\boldsymbol{\lambda}(t_k^+) \tag{23}$$

$$\boldsymbol{\lambda}(t_k^-) = \mathbf{Q}_k\mathbf{x}(t_k^-) + \mathbf{C}_k^{\mathsf{T}}\boldsymbol{\lambda}(t_k^+) \tag{24}$$

for which the relationship

$$\boldsymbol{\lambda}(t_k^{\pm}) = \mathbf{P}(t_k^{\pm})\mathbf{x}(t_k^{\pm}) \tag{25}$$

holds. After some manipulation of (23) and (24), it can be shown that

$$\mathbf{P}(t_k^-) = \mathbf{Q}_k + \mathbf{C}_k^{\mathsf{T}}\left(\mathbf{1} + \mathbf{P}(t_k^+)\mathbf{D}_k\mathbf{R}_k^{-1}\mathbf{D}_k^{\mathsf{T}}\right)^{-1}\mathbf{P}(t_k^+)\mathbf{C}_k \tag{26}$$

which is the well-known discrete-time matrix Riccati equation, but in this context it governs the instantaneous change in $\mathbf{P}$ across an impulse application time. The resulting matrix $\mathbf{P}(t_k^-)$ yields the boundary condition needed to integrate (22) backward on $[t_{k-1}^+, t_k^-]$.

Note that the discontinuity in the Riccati solution is consistent with the results of [19] who considered the case of a cost function with additional penalties on the states at discrete instants in time. This discontinuity does not appear to be part of the solution presented in [11].

The optimal feedback control laws for the continuous and impulsive inputs can now be written as

$$\mathbf{u}^*(t) = -\mathbf{R}^{-1}(t)\mathbf{B}^{\mathsf{T}}(t)\mathbf{P}(t)\mathbf{x}(t), \quad t \in \left[t_k^+, t_{k+1}^-\right] \tag{27}$$

$$\mathbf{v}_k^* = -\mathbf{R}_k^{-1}\mathbf{D}_k^{\mathsf{T}}\mathbf{C}_k^{-\mathsf{T}}\left(\mathbf{P}(t_k^-) - \mathbf{Q}_k\right)\mathbf{x}(t_k^-), \quad t = t_k^- \tag{28}$$

where (21) has been substituted into (19) and (24) has been solved for $\boldsymbol{\lambda}(t_k^+)$ and substituted into (20) for $\boldsymbol{\nu}_k$. Equations (27) and (28) are the optimal control inputs regardless of whether the optimal timing condition is satisfied or not. For the nonoptimal time, (27) and (28) are still optimal for the prescribed times.

C. Optimal Impulse Application Times

Let us briefly examine what (16) looks like for a continuous/discrete input linear, time-varying system governed by (1) and (2). For simplicity, it will be assumed for the duration of this paper that $\mathbf{C}_k$, $\mathbf{Q}_k$, and $\mathbf{R}_k$ are constant matrices. The preimpulse and postimpulse continuous Hamiltonians can be written as quadratic forms

$$\begin{aligned}\mathcal{H}_c(t_k^{\pm}) = {}& \frac{1}{2}\begin{bmatrix}\mathbf{x}(t_k^{\pm}) \\ \boldsymbol{\lambda}(t_k^{\pm})\end{bmatrix}^{\mathsf{T}}\begin{bmatrix}\mathbf{Q}(t_k^{\pm}) & \mathbf{A}^{\mathsf{T}}(t_k^{\pm}) \\ \mathbf{A}(t_k^{\pm}) & -\mathbf{B}(t_k^{\pm})\mathbf{R}^{-1}(t_k^{\pm})\mathbf{B}^{\mathsf{T}}(t_k^{\pm})\end{bmatrix} \\ & \cdot\left[\mathbf{x}^{\mathsf{T}}(t_k^{\pm}) \;\; \boldsymbol{\lambda}^{\mathsf{T}}(t_k^{\pm})\right]^{\mathsf{T}}.\end{aligned} \tag{29}$$

The transition of the states and costates from preimpulse to postimpulse, written in matrix form, is

$$\begin{bmatrix}\mathbf{x}(t_k^+) \\ \boldsymbol{\lambda}(t_k^+)\end{bmatrix} = \mathbf{G}_k\begin{bmatrix}\mathbf{x}(t_k^-) \\ \boldsymbol{\lambda}(t_k^-)\end{bmatrix} \tag{30}$$

where

$$\mathbf{G}_k = \begin{bmatrix}\mathbf{C}_k + \mathbf{D}_k\mathbf{R}_k^{-1}\mathbf{D}_k^{\mathsf{T}}\mathbf{C}_k^{-\mathsf{T}}\mathbf{Q}_k & -\mathbf{D}_k\mathbf{R}_k^{-1}\mathbf{D}_k^{\mathsf{T}}\mathbf{C}_k^{-\mathsf{T}} \\ -\mathbf{C}_k^{-\mathsf{T}}\mathbf{Q}_k & \mathbf{C}_k^{-\mathsf{T}}\end{bmatrix}. \tag{31}$$

Defining the matrices

$$\mathbf{H}_k^{\pm} = \begin{bmatrix}\mathbf{Q}(t_k^{\pm}) & \mathbf{A}^{\mathsf{T}}(t_k^{\pm}) \\ \mathbf{A}(t_k^{\pm}) & -\mathbf{B}(t_k^{\pm})\mathbf{R}^{-1}(t_k^{\pm})\mathbf{B}^{\mathsf{T}}(t_k^{\pm})\end{bmatrix} \tag{32}$$

and using (30), the postimpulse Hamiltonian, written in terms of the preimpulse states and costates, is

$$\mathcal{H}_c(t_k^+) = \frac{1}{2}\left[\mathbf{x}^{\mathsf{T}}(t_k^-) \;\; \boldsymbol{\lambda}^{\mathsf{T}}(t_k^-)\right]\mathbf{G}_k^{\mathsf{T}}\mathbf{H}_k^+\mathbf{G}_k\begin{bmatrix}\mathbf{x}(t_k^-) \\ \boldsymbol{\lambda}(t_k^-)\end{bmatrix}. \tag{33}$$

Finally, taking the partial derivative of (5) with respect to t_k, we get

$$\begin{aligned}\frac{\partial\mathcal{H}_{d,k}}{\partial t_k} &= \boldsymbol{\lambda}^{\mathsf{T}}(t_k^+)\frac{\partial\mathbf{D}_k}{\partial t_k}\mathbf{v}_k \\ &= -\boldsymbol{\lambda}^{\mathsf{T}}(t_k^+)\frac{\partial\mathbf{D}_k}{\partial t_k}\mathbf{R}_k^{-1}\mathbf{D}_k^{\mathsf{T}}\boldsymbol{\lambda}(t_k^+)\end{aligned} \tag{34}$$

assuming that $\mathbf{C}_k$, $\mathbf{Q}_k$, and $\mathbf{R}_k$ are constant.

Using (13), (15), and (20), and rewriting in matrix form, we obtain

$$\frac{\partial\mathcal{H}_{d,k}}{\partial t_k} = -\begin{bmatrix}\mathbf{x}(t_k^-) \\ \boldsymbol{\lambda}(t_k^-)\end{bmatrix}^{\mathsf{T}}\mathbf{F}_k\begin{bmatrix}\mathbf{x}(t_k^-) \\ \boldsymbol{\lambda}(t_k^-)\end{bmatrix}. \tag{35}$$

where we define the matrix $\mathbf{F}_k$ as

$$\mathbf{F}_k = -\begin{bmatrix} -\mathbf{Q}_k\mathbf{C}_k^{-1} \\ \mathbf{C}_k^{-1} \end{bmatrix} \frac{\partial \mathbf{D}_k}{\partial t_k} \mathbf{R}_k^{-1} \mathbf{D}_k^{\mathsf{T}} \begin{bmatrix} -\mathbf{C}_k^{-\mathsf{T}}\mathbf{Q}_k & \mathbf{C}_k^{-\mathsf{T}} \end{bmatrix}. \quad (36)$$

Using $\boldsymbol{\lambda}(t_k^-) = \mathbf{P}(t_k^-)\mathbf{x}(t_k^-)$, the extremal condition, (16), can be written in terms of only the preimpulse state vector as

$$\Delta_k = \frac{1}{2}\mathbf{x}^{\mathsf{T}}(t_k^-)\mathbf{M}_k\mathbf{x}(t_k^-) = 0 \quad (37)$$

where

$$\mathbf{M}_k = \mathbf{Y}_k^{\mathsf{T}}\left(\mathbf{H}_k^- - \mathbf{G}_k^{\mathsf{T}}\mathbf{H}_k^+\mathbf{G}_k + \mathbf{F}_k + \mathbf{F}_k^{\mathsf{T}}\right)\mathbf{Y}_k \quad (38)$$

and

$$\mathbf{Y}_k = \begin{bmatrix} \mathbf{1} & \mathbf{P}(t_k^-) \end{bmatrix}^{\mathsf{T}}.$$

There are three ways in which $\Delta_k = 0$ can be satisfied:

1) $\mathbf{x}(t_k^-) = \mathbf{0}$;
2) $\mathbf{M}_k = \mathbf{0}$;
3) $\mathbf{x}(t_k^-) \in \text{Null}(\mathbf{M}_k)$.

D. Sufficiency Condition

Determining an impulse time t_k that satisfies (16) can result in minimizing or maximizing J. In what follows, a sufficiency condition is derived for determining a minimum J with respect to t_k. For a local minimum of J, it suffices to show $d^2J \geq 0$ where

$$\begin{aligned} d^2J = \sum_{k=1}^{N-1} \Bigg\{ \Bigg(& \frac{\partial \mathcal{H}_c^-}{\partial t_k}dt_k + \frac{\partial \mathcal{H}_c^-}{\partial \mathbf{x}}^{\mathsf{T}} d\mathbf{x}^- + \frac{\partial \mathcal{H}_c^-}{\partial \mathbf{u}}^{\mathsf{T}} d\mathbf{u}^- \\ & + \frac{\partial \mathcal{H}_c^-}{\partial \boldsymbol{\lambda}}^{\mathsf{T}} d\boldsymbol{\lambda}^- - \frac{\partial \mathcal{H}_c^+}{\partial t_k}dt_k - \frac{\partial \mathcal{H}_c^+}{\partial \mathbf{x}}^{\mathsf{T}} d\mathbf{x}^+ \\ & - \frac{\partial \mathcal{H}_c^+}{\partial \mathbf{u}}^{\mathsf{T}} d\mathbf{u}^+ - \frac{\partial \mathcal{H}_c^+}{\partial \boldsymbol{\lambda}}^{\mathsf{T}} d\boldsymbol{\lambda}^+ \Bigg) dt_k \\ & + \frac{\partial^2 \mathcal{H}_{d,k}}{\partial t_k^2}dt_k^2 + 2\frac{\partial^2 \mathcal{H}_{d,k}}{\partial t_k \partial \mathbf{v}_k^{\mathsf{T}}}d\mathbf{v}_k dt_k + \frac{\partial^2 \mathcal{H}_{d,k}}{\partial t_k \partial \boldsymbol{\lambda}^{\mathsf{T}}}d\boldsymbol{\lambda}^+ dt_k \\ & + d\boldsymbol{\lambda}^{+\mathsf{T}}\frac{\partial^2 \mathcal{H}_{d,k}}{\partial \boldsymbol{\lambda} \partial \mathbf{v}_k^{\mathsf{T}}}d\mathbf{v}_k + d\boldsymbol{\lambda}^{+\mathsf{T}}\mathbf{C}_k d\mathbf{x}^- \\ & + d\mathbf{x}^{-\mathsf{T}}\mathbf{Q}_k d\mathbf{x}^- + d\mathbf{v}_k^{\mathsf{T}}\mathbf{R}_k d\mathbf{v}_k - d\boldsymbol{\lambda}^{-\mathsf{T}} d\mathbf{x}^- \Bigg\} \\ + \sum_{k=0}^{N} \int_{t_k^+}^{t_{k+1}^-} \Bigg[& \delta\mathbf{x}^{\mathsf{T}}(t)\left(\frac{\partial^2 \mathcal{H}_c(t)}{\partial \mathbf{x} \partial \mathbf{x}^{\mathsf{T}}}\delta\mathbf{x}(t) + 2\frac{\partial^2 \mathcal{H}_c(t)}{\partial \mathbf{x} \partial \mathbf{u}^{\mathsf{T}}}\delta\mathbf{u}(t)\right) \\ & + \delta\mathbf{u}^{\mathsf{T}}(t)\frac{\partial^2 \mathcal{H}_c(t)}{\partial \mathbf{u} \partial \mathbf{u}^{\mathsf{T}}}\delta\mathbf{u}(t) \Bigg] dt \end{aligned} \quad (39)$$

where the superscripts $(\cdot)^+$ and $(\cdot)^-$ have been used to denote the arguments (t_k^+) and (t_k^-).

The notation $(\cdot)' = d(\cdot)/dt_k$ is defined. Note that $(d(\cdot)/dt_k) \neq (d(\cdot)/dt)$. The derivative with respect to t_k is how a function changes with respect to the impulsive dynamics application time. For the case where the impulsive dynamics contain some feedback control, that change is not necessarily the same as how the function changes with respect to time. The relationships for the differentials of the states, costates, and controls are

$$\begin{aligned} d\mathbf{x}(t_k^\pm) &= \delta\mathbf{x}(t_k^\pm) + \mathbf{x}'(t_k^\pm)dt_k \\ d\boldsymbol{\lambda}(t_k^\pm) &= \delta\boldsymbol{\lambda}(t_k^\pm) + \boldsymbol{\lambda}'(t_k^\pm)dt_k \\ d\mathbf{u}(t_k^\pm) &= \delta\mathbf{u}(t_k^\pm) + \mathbf{u}'(t_k^\pm)dt_k \\ d\mathbf{v}_k &= \delta\mathbf{v}_k + \mathbf{v}_k' dt_k \end{aligned}$$

where $\delta\boldsymbol{\lambda}(t_k^\pm) = \mathbf{0}$. In addition, the differential of the postimpulse costate is related to its preimpulse counterpart by

$$d\boldsymbol{\lambda}^- = \mathbf{C}_k^{\mathsf{T}} d\boldsymbol{\lambda}^+ + \mathbf{Q}_k d\mathbf{x}^-. \quad (40)$$

It has been shown that the optimal continuous and impulsive inputs are identical to the optimal inputs for the classic continuous and discrete LQR problems, respectively. The optimal timing condition is an independent, additional condition. Therefore, it is valid to claim that

$$\begin{aligned} \min_{\mathbf{u},\mathbf{v}_k,t_k} J(\mathbf{u},\mathbf{v}_k,t_k) &= \min_{t_k} \min_{\mathbf{u},\mathbf{v}_k} J(\mathbf{u},\mathbf{v}_k,t_k) \\ &= \min_{t_k} J\left(\mathbf{u}^*,\mathbf{v}_k^*,t_k\right). \end{aligned}$$

Like its classical counterparts, a sufficient condition for a minimum of the hybrid cost function with respect to the inputs is the Legendre–Clebsch condition for both sets of inputs, i.e., $\partial^2\mathcal{H}_c/\partial\mathbf{u}\partial\mathbf{u}^{\mathsf{T}} > \mathbf{0}$, $\partial^2\mathcal{H}_{d,k}/\partial\mathbf{v}_k\partial\mathbf{v}_k^{\mathsf{T}} > \mathbf{0}$. As in the case of the necessary conditions, there remains a second, input-independent sufficient condition for a minimum with respect to application time.

By prescribing the optimal control inputs, the variations of the control inputs, and consequently the state, vanish. What remains yields the sufficient condition for a minimum with respect to application time

$$\begin{aligned} d^2J = \sum_{k=1}^{N-1} \Bigg[& \frac{\partial \mathcal{H}_c^-}{\partial t_k} + \frac{\partial \mathcal{H}_c^-}{\partial \mathbf{x}}^{\mathsf{T}} \mathbf{x}'(t_k^-) + \frac{\partial \mathcal{H}_c^-}{\partial \mathbf{u}}^{\mathsf{T}} \mathbf{u}'(t_k^-) \\ & + \frac{\partial \mathcal{H}_c^-}{\partial \boldsymbol{\lambda}}^{\mathsf{T}} \boldsymbol{\lambda}'(t_k^-) - \frac{\partial \mathcal{H}_c^+}{\partial t_k} - \frac{\partial \mathcal{H}_c^+}{\partial \mathbf{x}}^{\mathsf{T}} \mathbf{x}'(t_k^+) \\ & - \frac{\partial \mathcal{H}_c^+}{\partial \mathbf{u}}^{\mathsf{T}} \mathbf{u}'(t_k^+) - \frac{\partial \mathcal{H}_c^+}{\partial \boldsymbol{\lambda}}^{\mathsf{T}} \boldsymbol{\lambda}'(t_k^+) + \frac{\partial^2 \mathcal{H}_{d,k}}{\partial t_k^2} \\ & + 2\frac{\partial^2 \mathcal{H}_{d,k}}{\partial t_k \partial \mathbf{v}_k^{\mathsf{T}}}\mathbf{v}_k' + \frac{\partial^2 \mathcal{H}_{d,k}}{\partial t_k \partial \boldsymbol{\lambda}^{\mathsf{T}}}\boldsymbol{\lambda}'(t_k^+) \\ & + \boldsymbol{\lambda}'^{\mathsf{T}}(t_k^+)\frac{\partial^2 \mathcal{H}_{d,k}}{\partial \boldsymbol{\lambda} \partial \mathbf{v}_k^{\mathsf{T}}}\mathbf{v}_k' + \mathbf{v}_k'^{\mathsf{T}}\mathbf{R}_k\mathbf{v}_k' \Bigg] dt_k^2 \geq 0. \end{aligned} \quad (41)$$

It is observed that the sum of the various partial derivative terms of the continuous Hamiltonian is equal to the full derivative of the continuous Hamiltonian with respect to t_k

$$\frac{d\mathcal{H}_c}{dt_k} = \frac{\partial \mathcal{H}_c}{\partial t_k} + \frac{\partial \mathcal{H}_c}{\partial \mathbf{x}}^{\mathsf{T}} \frac{d\mathbf{x}}{dt_k} + \frac{\partial \mathcal{H}_c}{\partial \mathbf{u}}^{\mathsf{T}} \frac{d\mathbf{u}}{dt_k} + \frac{\partial \mathcal{H}_c}{\partial \boldsymbol{\lambda}}^{\mathsf{T}} \frac{d\boldsymbol{\lambda}}{dt_k} \quad (42)$$

such that d^2J can be written as

$$\begin{aligned} d^2J &= \sum_{k=1}^{N-1}\Bigg[\frac{d\mathcal{H}_c^-}{dt_k}-\frac{d\mathcal{H}_c^+}{dt_k}+\frac{\partial^2\mathcal{H}_{d,k}}{\partial t_k^2}+2\frac{\partial^2\mathcal{H}_{d,k}}{\partial t_k\partial\mathbf{v}_k^\mathsf{T}}\mathbf{v}_k' \\ &\quad+\frac{\partial^2\mathcal{H}_{d,k}}{\partial t_k\partial\boldsymbol{\lambda}^\mathsf{T}}\boldsymbol{\lambda}'\big(t_k^+\big)+\boldsymbol{\lambda}'^\mathsf{T}\big(t_k^+\big)\frac{\partial^2\mathcal{H}_{d,k}}{\partial\boldsymbol{\lambda}\partial\mathbf{v}_k^\mathsf{T}}\mathbf{v}_k'+\mathbf{v}_k'^\mathsf{T}\mathbf{R}_k\mathbf{v}_k'\Bigg]dt_k^2. \end{aligned} \tag{43}$$

From the definition of $\mathcal{H}_{d,k}$ in (5), we note that

$$\frac{\partial^2\mathcal{H}_{d,k}}{\partial\boldsymbol{\lambda}\partial\mathbf{v}_k^\mathsf{T}}=\mathbf{D}_k,\quad \frac{\partial^2\mathcal{H}_{d,k}}{\partial t_k\partial\mathbf{v}_k^\mathsf{T}}=\boldsymbol{\lambda}^\mathsf{T}\big(t_k^+\big)\mathbf{D}_k' \tag{44}$$

and from the expression for the impulsive optimal control in (15) and (20) we have

$$\mathbf{v}_k'=-\mathbf{R}_k^{-1}\mathbf{D}_k'^\mathsf{T}\boldsymbol{\lambda}\big(t_k^+\big)-\mathbf{R}_k^{-1}\mathbf{D}_k^\mathsf{T}\boldsymbol{\lambda}'\big(t_k^+\big). \tag{45}$$

Using these expressions, it follows that:

$$\frac{\partial^2\mathcal{H}_{d,k}}{\partial t_k\partial\mathbf{v}_k^\mathsf{T}}\mathbf{v}_k'+\boldsymbol{\lambda}'^\mathsf{T}\big(t_k^+\big)\frac{\partial^2\mathcal{H}_{d,k}}{\partial\boldsymbol{\lambda}\partial\mathbf{v}_k^\mathsf{T}}\mathbf{v}_k'+\mathbf{v}_k'^\mathsf{T}\mathbf{R}_k\mathbf{v}_k'=\mathbf{0}. \tag{46}$$

Also

$$\frac{d}{dt_k}\left(\frac{\partial\mathcal{H}_{d,k}}{\partial t_k}\right)=\frac{\partial^2\mathcal{H}_{d,k}}{\partial t_k^2}+\frac{\partial^2\mathcal{H}_{d,k}}{\partial t_k\partial\mathbf{v}_k^\mathsf{T}}\mathbf{v}_k'+\frac{\partial^2\mathcal{H}_{d,k}}{\partial t_k\partial\boldsymbol{\lambda}^\mathsf{T}}\boldsymbol{\lambda}'\big(t_k^+\big) \tag{47}$$

which when combined with the result in (46) allows (43) to be written as

$$d^2J=\sum_{k=1}^{N-1}\frac{d}{dt_k}\Big(\mathcal{H}_c\big(t_k^-\big)-\mathcal{H}_c\big(t_k^+\big)+\frac{\partial\mathcal{H}_d}{\partial t_k}\Big)dt_k^2. \tag{48}$$

Therefore, sufficient conditions for a local minimum with respect to the application time of the impulsive dynamics can be written as

$$\Delta_k^2\equiv\frac{d}{dt_k}\Big(\mathcal{H}_c\big(t_k^-\big)-\mathcal{H}_c\big(t_k^+\big)+\frac{\partial\mathcal{H}_{d,k}}{\partial t_k}\Big)\geq 0 \tag{49}$$

for each application time $k=1,\ldots,N-1$. Simple numerical examples that validated the optimality conditions in (16) and (49) were presented in [12].

III. Application to Lorentz-Augmented Formation Flight

A. Formation Flight Dynamics

We consider a two-spacecraft formation where one of the vehicles is designated as the chief and it is left uncontrolled. The other vehicle is termed the deputy and it is subject to the Lorentz force (described below) and the additional impulsive thrusting. The mean differential element error dynamics, first introduced by Schaub *et al.* [20], and subsequently used successfully for other formation controller designs [6], [8], are chosen to model the relative error dynamics of the deputy spacecraft of the two-spacecraft formation.

Although not as important for the formation reconfiguration problem as it is for formation keeping, the mean elements include the secular effect of the J_2 zonal harmonic in the dynamics. It will be seen that Lorentz-augmented transfers can take a considerable amount of time, so the secular effects of J_2 on the orbits will not be negligible. The mean differential element error dynamics are also LTV dynamics and lend themselves well to the design of a continuous/impulsive LQR controller.

In Section III-C, a feedback controller will be designed by applying the theory of Section II to the mean element description of the reconfiguration error dynamics which is, essentially, a regulator problem. We defend the choice of the mean elements by noting the following passage from [20]: dealing with mean orbit elements has the advantage that short period oscillations are not perceived as tracking error; rather, only the long term tracking errors are compensated for. By feeding back errors in mean elements, advantage is taken of celestial mechanics insight to avoid trying to correct orbit elements at ill-suited times.

The classical (osculating) orbital elements are $\boldsymbol{e}=[a\,e\,i\,\Omega\,\omega\,M]^\mathsf{T}$, where a is the semimajor axis, e is the eccentricity, i is the inclination, Ω is the right ascension of the ascending node, ω is the argument of periapsis, and M is the mean anomaly. The classical mean orbital element set is $\bar{\boldsymbol{e}}=[\bar{a}\;\bar{e}\;\bar{i}\;\bar{\Omega}\;\bar{\omega}\;\bar{M}]^\mathsf{T}$, where mean orbital elements are denoted by the $\bar{(\cdot)}$ notation. The mappings from the osculating elements to the mean elements are presented in [21].

Let the mean differential element error be

$$\begin{aligned}\mathbf{x}(t)&=\bar{\boldsymbol{e}}_d(t)-\bar{\boldsymbol{e}}_r\\&=(\bar{\boldsymbol{e}}_d(t)-\bar{\boldsymbol{e}}_c(t))-(\bar{\boldsymbol{e}}_r-\bar{\boldsymbol{e}}_c(t))\\&=\delta\bar{\boldsymbol{e}}_d(t)-\delta\bar{\boldsymbol{e}}_r(t)\end{aligned} \tag{50}$$

where $\bar{\boldsymbol{e}}_c$ are the mean elements of the chief, $\bar{\boldsymbol{e}}_d$ are the mean elements of the deputy, the subscript $(\cdot)_r$ denotes the reference orbital elements of the desired formation ($\bar{\boldsymbol{e}}_r$ are the desired deputy mean elements), and $\delta\bar{\boldsymbol{e}}_d$ denotes the differential elements, those being the differences in orbital elements between the deputy and chief spacecraft. Thus, $\delta\bar{\boldsymbol{e}}_r$ denotes the difference between the reference mean element set and those of the chief.

The linearized continuous and discrete mean differential element error dynamics governing $\mathbf{x}$ are

$$\dot{\mathbf{x}}(t)=\mathbf{A}(\bar{\boldsymbol{e}}_r)\mathbf{x}(t)+\boldsymbol{\mathcal{B}}(t,\bar{\boldsymbol{e}}_r)\bar{\mathbf{u}}(t) \tag{51}$$

$$\mathbf{x}\big(t_k^+\big)=\mathbf{x}\big(t_k^-\big)+\boldsymbol{\mathcal{B}}\big(t_k^-,\bar{\boldsymbol{e}}_r\big)\mathbf{v}_k \tag{52}$$

where the input matrix $\boldsymbol{\mathcal{B}}$ contains Gauss's variational equations [22]

$$\begin{aligned}&\boldsymbol{\mathcal{B}}(t,\boldsymbol{e})\\&=\begin{bmatrix}\frac{2a^2e\sin f}{h} & \frac{2a^2p}{rh} & 0\\ \frac{p\sin f}{h} & \frac{(p+r)\cos f+re}{h} & 0\\ 0 & 0 & \frac{r\cos\theta}{h}\\ 0 & 0 & \frac{r\sin\theta}{h\sin i}\\ -\frac{p\cos f}{he} & \frac{(p+r)\sin f}{he} & -\frac{r\sin\theta}{h\tan i}\\ \frac{b(p\cos f-2re)}{ahe} & -\frac{b(p+r)\sin f}{ahe} & 0\end{bmatrix}.\end{aligned} \tag{53}$$

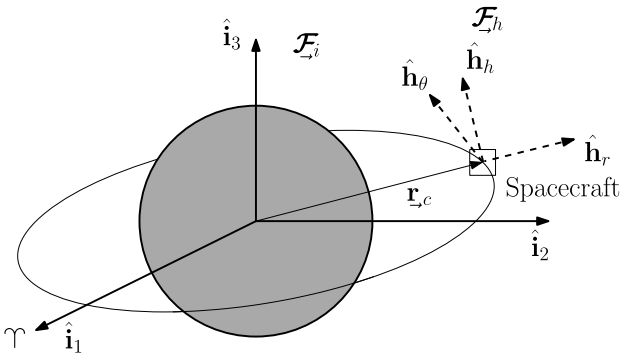

Fig. 1. LVLH frame.

where h is the orbit's specific angular momentum, r is the orbit radius, b is the orbit's semiminor axis, p is the semilatus rectum, f is the true anomaly, and $\theta = \omega + f$ is the true latitude.

The continuous state matrix is

$$\mathbf{A}(\bar{\boldsymbol{e}}_r) = \left[\begin{array}{ccc|c} \multicolumn{3}{c|}{\mathbf{0}_{3\times 3}} & \mathbf{0}_{3\times 3} \\ \hline \frac{\partial \dot{\bar{\Omega}}}{\partial \bar{a}} & \frac{\partial \dot{\bar{\Omega}}}{\partial \bar{e}} & \frac{\partial \dot{\bar{\Omega}}}{\partial \bar{i}} & \\ \frac{\partial \dot{\bar{\omega}}}{\partial \bar{a}} & \frac{\partial \dot{\bar{\omega}}}{\partial \bar{e}} & \frac{\partial \dot{\bar{\omega}}}{\partial \bar{i}} & \mathbf{0}_{3\times 3} \\ \frac{\partial \dot{\bar{M}}}{\partial \bar{a}} & \frac{\partial \dot{\bar{M}}}{\partial \bar{e}} & \frac{\partial \dot{\bar{M}}}{\partial \bar{i}} & \end{array}\right]. \tag{54}$$

The secular mean element drift rates, $\dot{\bar{\Omega}}$, $\dot{\bar{\omega}}$, and $\dot{\bar{M}}$ and their partial derivatives can be found in [21]. The vector $\bar{\mathbf{u}}(t)$ in (51) and the vector $\mathbf{v}_k$ in (52) are the applied continuous acceleration and impulsive thrust, respectively, and are expressed in the spacecraft's local-vertical local-horizontal (LVLH) frame, where the vector $\hat{\mathbf{h}}_r$ is in the direction of the chief's orbital radius, $\hat{\mathbf{h}}_h$ is aligned with the chief's angular momentum vector, and the vector $\hat{\mathbf{h}}_\theta$ completes the right-hand rule, as illustrated in Fig. 1. The origin of the LVLH frame is located at the chief spacecraft.

We are interested in utilizing the geomagnetic Lorentz force as the primary means of propulsion for a spacecraft for the purpose of spacecraft formation reconfiguration. This would require a spacecraft to carry and modulate a significant electrical charge. Any spacecraft with a net electrical charge and a nonzero velocity relative to the earth's magnetic field will experience the Lorentz force, which, per unit mass is given by

$$\vec{\mathbf{f}}_L(t) = \frac{q(t)}{m} \underbrace{\left(\dot{\vec{\mathbf{r}}}(t) - \vec{\boldsymbol{\omega}}_\oplus \times \vec{\mathbf{r}}(t)\right) \times \vec{\mathbf{b}}_\oplus(t)}_{\equiv \tilde{\vec{\mathbf{f}}}_L}. \tag{55}$$

The quantity q/m is the charge-to-mass ratio, or specific charge, $\vec{\mathbf{b}}_\oplus$ is the local magnetic field vector of the earth, $\vec{\boldsymbol{\omega}}_\oplus$ is the angular velocity vector of the earth, and $\vec{\mathbf{r}}$ and $\dot{\vec{\mathbf{r}}}$ are the spacecraft position and velocity vectors, respectively.

For a Lorentz-augmented spacecraft, the continuous acceleration is given by

$$\bar{\mathbf{u}}(t) = \frac{q(t)}{m} \mathbf{C}_{hi} \tilde{\mathbf{f}}_L \tag{56}$$

where $\mathbf{C}_{hi}$ is the rotation matrix from the geocentric inertial frame, $\vec{\mathcal{F}}_i$, to the LVLH frame, $\vec{\mathcal{F}}_h$, of the reference orbit, and the quantity $\tilde{\mathbf{f}}_L$ are the components expressed in $\vec{\mathcal{F}}_i$ of the vector $\tilde{\vec{\mathbf{f}}}_L(t)$ defined in (55). The sole continuous control input $u(t)$ is the specific charge $q(t)/m$. Therefore, upon substituting (56) into (51), (51) becomes

$$\dot{\mathbf{x}}(t) = \mathbf{A}(\bar{\boldsymbol{e}}_r)\mathbf{x}(t) + \underbrace{\left(\boldsymbol{\mathcal{B}}(t, \bar{\boldsymbol{e}}_r)\mathbf{C}_{hi}\tilde{\mathbf{f}}_L\right)}_{\equiv \mathbf{B}(t, \bar{\boldsymbol{e}}_r)} u(t). \tag{57}$$

Note that (57) can be identified with (1) and (52) can be identified with (2) with $\mathbf{C}_k = \mathbf{1}$ and $\mathbf{D}_k = \boldsymbol{\mathcal{B}}(t_k^-, \bar{\boldsymbol{e}}_r)$. In [8] and [9], an analysis of the controllability of the Lorentz-augmented differential element dynamics revealed that the controllable subspace has dimension five in a state space of dimension six, which motivates the need for the additional thruster actuation. The design goal for the continuous/discrete LQR is to minimize the required thruster effort required for the Lorentz-augmented maneuvers.

B. Optimal Formation Reconfiguration Problem

Given a set of chief mean orbital elements $\bar{\boldsymbol{e}}_c$ and an initial formation described by the deputy mean orbital elements $\bar{\boldsymbol{e}}_d(0)$, we wish to transfer the mean differential deputy elements close to a formation $\delta\bar{\boldsymbol{e}}_r$ in finite time. In other words, the objective is to transfer the state in (50) from $\mathbf{x}(0) = \bar{\boldsymbol{e}}_d(0) - \bar{\boldsymbol{e}}_r$ to a state $\mathbf{x}(t) = \bar{\boldsymbol{e}}_d(t) - \bar{\boldsymbol{e}}_r$ in some neighborhood of the origin. We will be using the hybrid feedback regulator solution developed in Section II to transfer the deputy's relative mean element error to a vicinity of the origin in finite time. This can be effectively accomplished by determining u using (27), $\mathbf{v}_k$ using (28), and t_k, $k = 1, \ldots, N-1$, using (16), (37), and (38), which minimizes the performance index in (3). The selection of the weighting matrices appearing there is discussed in Section III-D.

C. Algorithm for Optimal Time Determination

The optimally timed hybrid LQR is applied to the formation reconfiguration problem in the following manner. There is no prescribed time limit on the duration of the reconfiguration, nor is the duration of the reconfiguration penalized. Because the theory does not indicate what the optimal number of thrusts is and there is no specific duration for the maneuver, one thrust (albeit, optimally timed) is applied per orbit. Furthermore, the case of no thrust being applied in a specific orbit is not considered. Given the complex dependence of the deputy spacecraft tracking error on the design parameters, the reconfiguration maneuver is terminated once a periodic, steady-state error is observed.

Determining the optimal impulse application times is not particularly straightforward. From (37) and (38), it is evident that the condition requires both the solution of the Riccati equation (which is integrated backward) and to the state (which is integrated forward and depends on the Riccati solution) at $t = t_k^-$. This is problematic, since each impulse application will result in a different solution to the Riccati equations and each new Riccati solution results in a different state trajectory.

TABLE I
INITIAL AND TARGET ORBITAL ELEMENTS FOR 10–1 km RECONFIGURATION

Chief elements			Deputy initial diff. elements			Deputy target diff. elements	
	unit	quantity		unit	quantity	unit	quantity
$\bar{a}$	km	7092	$\delta\bar{a}$	m	0.542	m	-1.836
$\bar{e}$		0.05	$\delta\bar{e}$	– 10^{-4}	-4.985	– 10^{-10}	8.572
$\bar{i}$	deg	90.0	$\delta\bar{i}$	deg, 10^{-2}	5.593	deg, 10^{-3}	7.973
$\bar{\Omega}$	deg	0.0	$\delta\bar{\Omega}$	deg, 10^{-2}	-5.453	deg, 10^{-3}	0.0
$\bar{\omega}$	deg	0.003	$\delta\bar{\omega}$	deg, 10^{-1}	-5.713	deg, 10^{-2}	-8.060
$\bar{M}$	deg	359.997	$\delta\bar{M}$	deg, 10^{-1}	5.706	deg, 10^{-2}	8.050

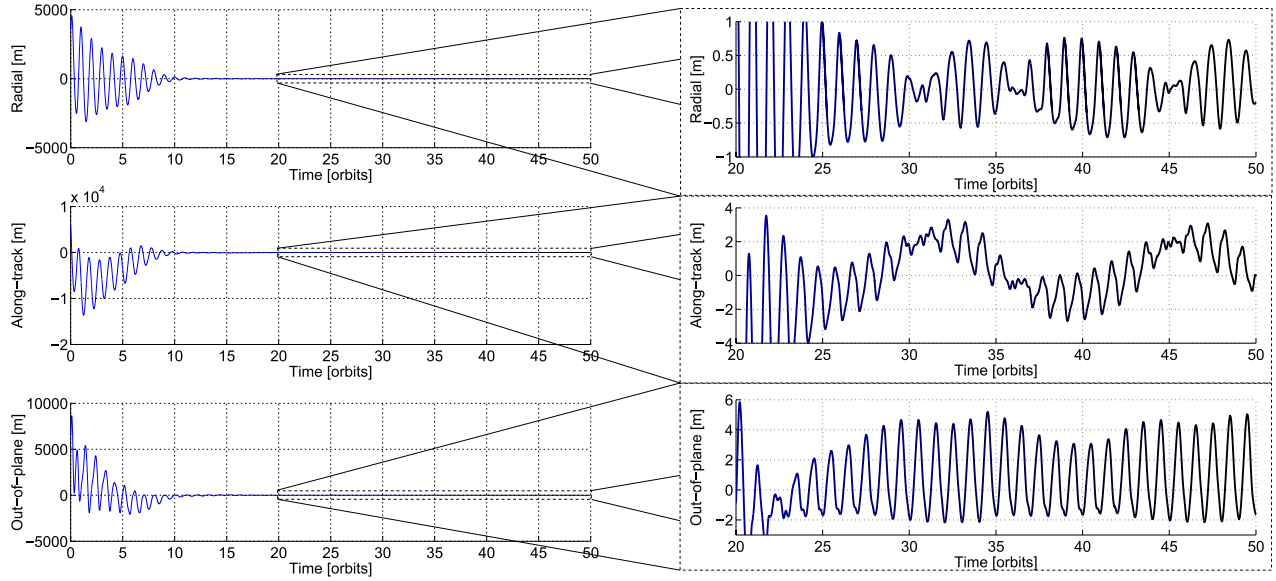

Fig. 2. Relative position error of deputy spacecraft during reconfiguration in the LVLH frame.

To properly evaluate (37) at an assumed value of t_k, one first needs to calculate the full solution to the continuous Riccati equation over the control interval, including the jump in the solution (occurring at the assumed value of t_k) determined using the discrete Riccati equation, and then integrate the state equations with the feedback control forward in time to $t = t_k$ to obtain the state $\mathbf{x}(t_k^-)$. To determine an optimal t_k, a control interval must be discretized and at each node one tests the corresponding value of t_k by checking the optimality conditions using the procedure just discussed.

For the results that will be presented, one orbit at a time was considered a control period. Hence, the hybrid optimal control solution in Section II is applied over successive time windows with $t = t_0$ identified with the beginning of the orbit and $t = t_f = t_0 + T$ identified with the end of the orbit (T is the orbital period). The following algorithm was used to implement the optimal impulse application time for one orbit at a time.

1) For a given initial differential element error, $\mathbf{x}(t_0)$, determine an optimal impulse application time $t_k = t_1 \in [t_0, t_0 + T]$ using the above procedure, and calculate the corresponding solution to the Riccati equation on $[t_0, t_0 + T]$ for that choice of impulse application time.
2) Simulate the formation for this orbit, from $t = t_0$ to $t = t_0 + T$, using the optimally timed hybrid LQR solution for that orbit by applying the feedback solutions in (27) and (28) with the impulse application time $t_k = t_1$ determined in step 1 to satisfy the optimality condition in (37). This simulation in step 2 for the real behavior of the formation needs to be distinguished from the offline one required in step 1 to determine the optimal value of $t_k = t_1$.
3) Calculate the new differential element error after one orbit, $\mathbf{x}(t_0 + T)$ and set t_0 to $t_f = t_0 + T$ while returning to step 1. Repeat until reconfiguration is complete.

It is possible that on a finite time interval of one orbit, $t_0 \le t \le t_0 + T$, there is no time t_k at which the optimality conditions (16) and (49) are satisfied. If that is the case, then the minimum for that time interval is at one of the end points. This is taken into account when determining the optimal application time for each orbit.

D. Numerical Example

The reconfiguration example we consider is a deputy spacecraft transferring from a 10-km projected circular orbit (PCO), with a phase angle of $\alpha_0 = \pi/4$ rad to a 1-km PCO with $\alpha_0 = 0$ rad. The initial conditions of both chief and deputy spacecraft, as well as the reference elements are given in Table I. The mapping from Cartesian relative position to differential elements can be found in [23]. The formation is in a low earth orbit with a semimajor axis of 7092 km (orbital period of $T = 5956$ s), eccentricity of 0.05 and an inclination of 90° (these are the chief's mean elements).

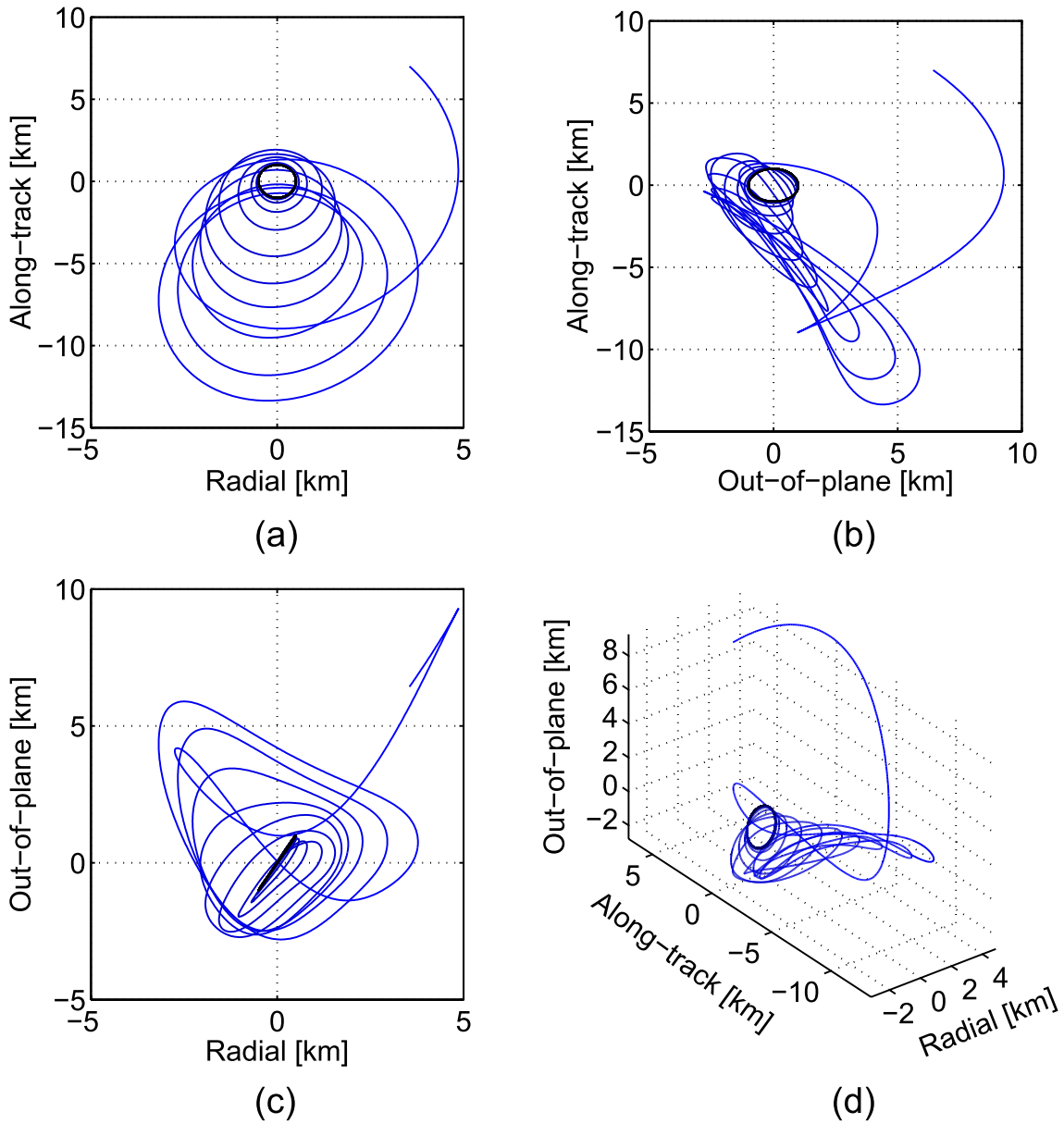

Fig. 3. Trajectory of deputy spacecraft transferring from a 10-km PCO to a 1-km PCO as seen in the LVLH frame. (a) Radial along-track plane. (b) Radial out-of-plane plane. (c) Along-track out-of-plane plane. (d) Trajectory in the LVLH frame.

The mapping from the Cartesian relative motion description to differential elements can be found in [21].

For the numerical simulation, the nonlinear inertial equations of motion of the chief and deputy spacecraft are integrated. The gravity model used includes J_2–J_6 zonal harmonics and the magnetic field model used is the IGRF-11 model [24].

To minimize the usage of impulsive actuation, the state penalty weights of the continuous/impulsive LQR are chosen based on the controllability Gramian of the Lorentz-augmented differential element error dynamics (57). The impulsive state penalty matrix, $\mathbf{Q}_k$ is chosen to be

$$\mathbf{Q}_k = C_2 \boldsymbol{\eta}_0 \boldsymbol{\eta}_0^{\mathsf{T}} \tag{58}$$

where $\boldsymbol{\eta}_0$ is the eigenvector of the controllability Gramian associated with the zero eigenvalue of the Gramian and C_2 is a scaling parameter. This effectively restricts the impulsive control effort to only targeting the portion of the state that cannot be corrected by the Lorentz force.

The continuous state penalty matrix $\mathbf{Q}$ is calculated using the remaining eigenvectors of the Gramian

$$\mathbf{Q} = C_1[\boldsymbol{\eta}_1\ \boldsymbol{\eta}_2\ \boldsymbol{\eta}_3\ \boldsymbol{\eta}_4\ \boldsymbol{\eta}_5][\boldsymbol{\eta}_1\ \boldsymbol{\eta}_2\ \boldsymbol{\eta}_3\ \boldsymbol{\eta}_4\ \boldsymbol{\eta}_5]^{\mathsf{T}} \tag{59}$$

where C_1 is again a scaling parameter (the Gramian is calculated by integrating over one period). The terminal weighting matrix is taken to be $\mathbf{K} = \mathbf{0}$.

For the reconfiguration being considered, the scaling parameters are set to $C_1 = C_2 = 10^6$. The control effort penalty matrices are $R = 10^6$ and $\mathbf{R}_k = 10^8 \cdot \mathbf{1}_{3\times 3}$ for continuous and impulsive controls, respectively. Fig. 2 presents the components of relative position error of the reconfiguring spacecraft and the relative trajectory of the deputy spacecraft is shown in Fig. 3. Note that the resulting controller is not a particularly aggressive one: approximately 25 orbits

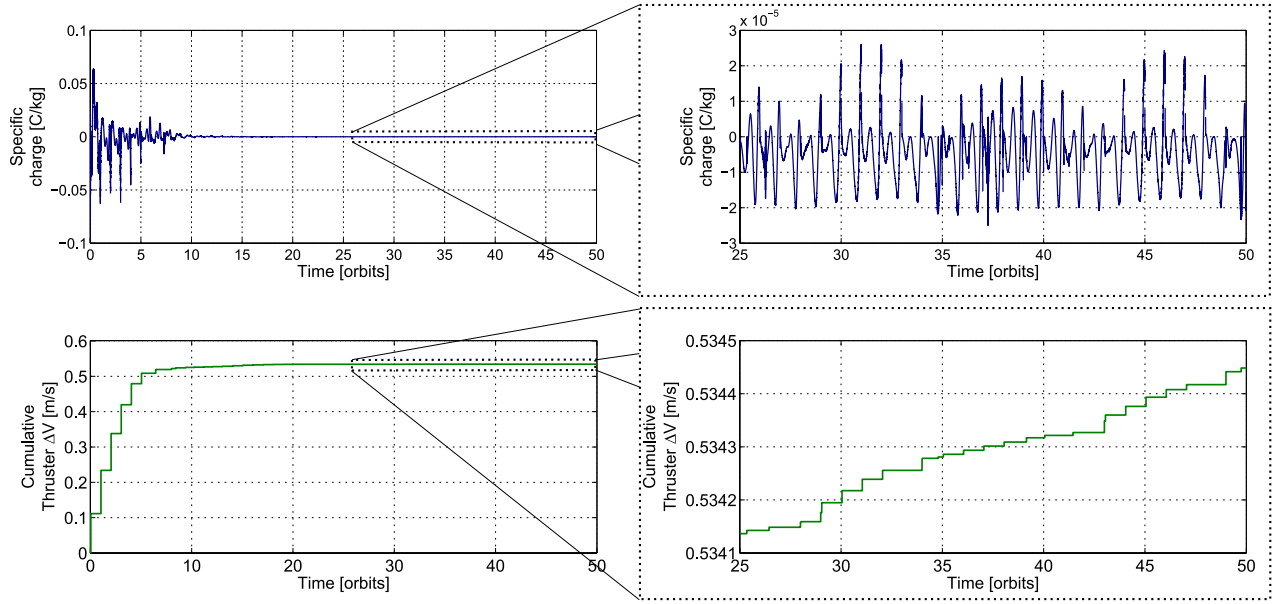

Fig. 4. Applied control efforts for a reconfiguration maneuver from a 10-km PCO to a 1-km PCO.

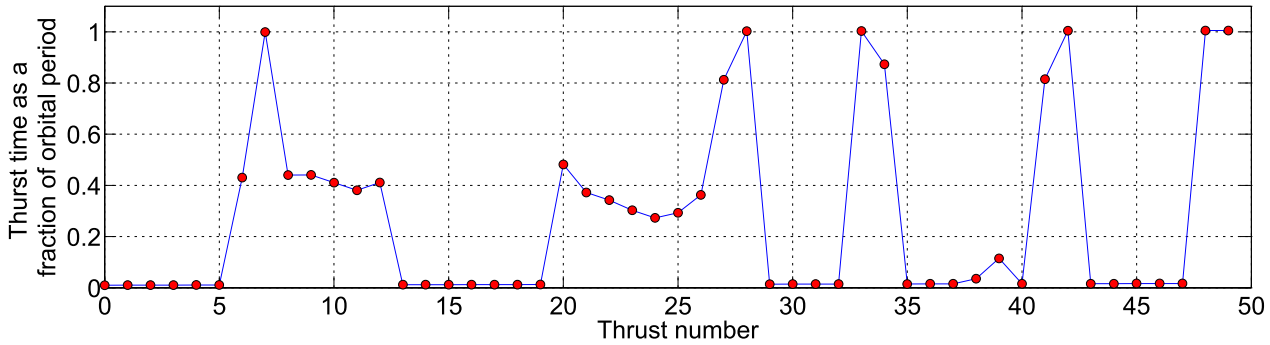

Fig. 5. Optimal reconfiguration thrust times for a 10-km PCO to a 1-km PCO.

are required to perform the desired maneuver, whereas a conventional impulsive transfer requires only a single orbit. A more aggressive control could be designed, but this will result in specific charge magnitudes that are considerably larger than what is currently considered to be feasible. What specific charge is feasible will be discussed in more detail later on.

The control effort required for this reconfiguration is given in Fig. 4. For the first seven orbits, the specific charge is of order 10^{-1}–10^{-2} C/kg; the rms specific charge for that period is 0.0148 C/kg. After seven orbits, the specific charge decreases to a magnitude on the order 10^{-3}–10^{-4} C/kg, eventually reaching a magnitude of order 10^{-5} C/kg.

Cumulative thruster control effort for the reconfiguration is 0.535 m/s which is calculated as the sum of the 2-norms of thrust vectors. Impulsive thrust magnitudes are largest during the first seven orbits, where they are have a magnitude of order 10^{-1} m/s. They reduce in magnitude to the order of 10^{-3} m/s and smaller for the remainder of the simulation. In comparison, a conventional two impulsive-thrust reconfiguration strategy requires a total ΔV of 15.1 m/s to perform the same maneuver, although such a maneuver takes only a single orbit. Fig. 4 plots the continuous and impulsive control efforts for the entire 50 orbit simulation.

The reconfiguration is completed after 25 orbits, after which the role of the controller becomes that of formation keeping in the presence of the J_2 perturbation. This can been observed in Fig. 2, where a time varying but steady-state position error is achieved in the latter half of the simulation. Impulsive and specific charge control efforts are similar to those seen for Lorentz-augmented formation keeping [8], however, now with optimized, rather than prescribed, impulse application times.

Fig. 5 plots each optimal thrust application time as a fraction of orbital period. Recall, in this example chief argument of perigee is $\omega = 0°$, so the beginning of the orbit corresponds to perigee while $t = 0.5$ nT, with n being number of completed orbits, corresponds to apogee. From Fig. 5, we see that optimal times for most orbits correspond with perigee: most times are either at the very beginning or very end of the orbital period. This is entirely consistent with the fact that the Lorentz force is nearly perpendicular to the spacecraft velocity vector. This ensures that for a nearly circular orbit, there will be little force impacting the differential semimajor axis coordinate and it will be nearly uncontrollable. Given the way in which the impulsive

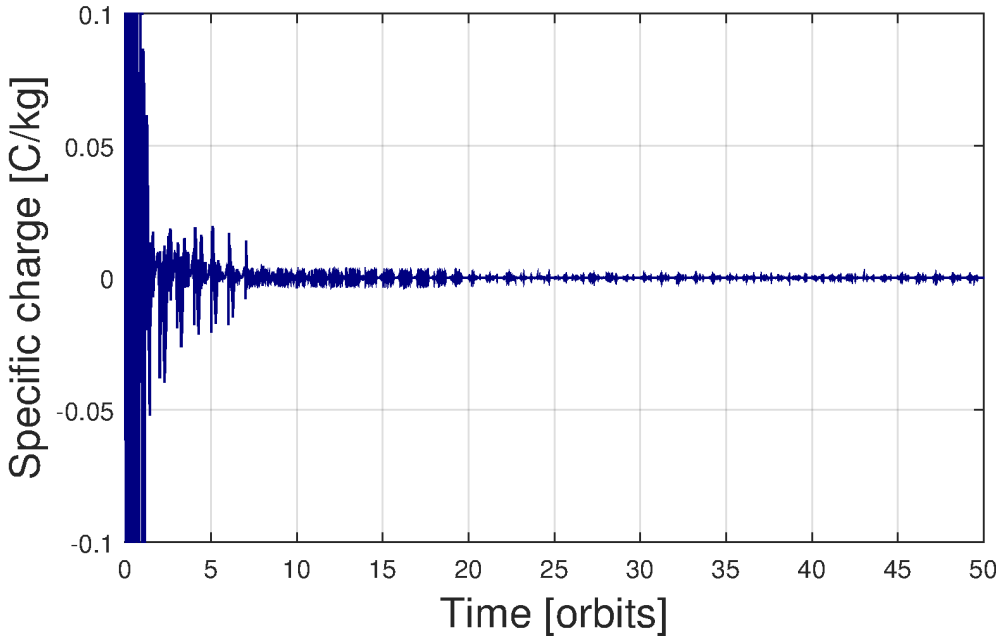

Fig. 6. Specific charge for case with navigation errors (±5 cm in relative position, ±1 mm in relative velocity).

state penalty matrix is selected in (58), it makes sense that the impulsive thrusts should occur to have maximum impact on the differential semimajor axis. In some cases, a thrust at the end of an orbit is followed by a thrust applied immediately at the start of the next orbit, suggesting that in those cases, the two thrusts can be combined into a single thrust.

It is possible that navigation errors (which were neglected in the previously presented results) could have a negative impact on the performance of our control scheme, in particular, propellant usage. In addition to the previous results, we have performed our simulations with uniformly distributed random noise added to the coordinates of the Cartesian relative state prior to conversion to differential mean elements. In particular, the relative Cartesian position had uniformly distributed errors (±5 cm) added and the relative Cartesian velocity had uniformly distributed errors (±1 mm/s) added. With the errors added, the specific charge experienced considerable saturation (at the maximum imposed charge level of 0.1 C/kg) during the earlier orbits (see Fig. 6). The time to steady-state error behavior remained at 25 orbits. The cumulative thruster Δv for the reconfiguration (over the first 25 orbits) was increased from 0.535 to 0.653 m/s.

During the steady-state period (the last 25 orbits) the cumulative thruster Δv increased to 0.0004 m/s from the original (error free) value of 0.0002 m/s and the rms charge increased to 1.63×10^{-5} from 1.25×10^{-5} C/kg. The steady-state rms errors in the relative Cartesian errors (calculated using the last 25 orbits) changed from from 0.574 to 0.363 m (radial), from 1.677 to 2.139 m (along track), and from 1.782 to 1.615 m (cross track). As can be seen, the uniformly distributed errors have only a small impact on the controller performance.

When the magnitude of the errors are increased to 50 cm and 1 cm/s the performance worsens considerably. In this case, the steady-state rms errors over the last 25 orbits increase to 1.534 m (radial), 11.05 m (along track), and 6.718 m (cross track). The rms specific charge over this time is 5.27×10^{-4} C/kg and the thruster Δv is comparable with the previous case (0.0004 m/s).

At this time, it is believed that through the adaptation of current technology, the maximum specific charge magnitudes that can be currently achieved are of order 10^{-3}–10^{-2} C/kg [1], [25]. Unfortunately, this puts the presented maneuver at the limit of what is believed to be feasible with existing technology. The proposed Lorentz-augmented spacecraft architecture in [26] is capable of specific charge magnitudes of order 10^{-3}, but the large size of the proposed spacecraft (mass 600 kg and length 20 km) makes it impractical for spacecraft formations. Considerable work remains to be done in determining feasible hardware for realizing Lorentz-augmented formation flight.

IV. Conclusion

A method for determining the optimal impulse application times for a continuous/impulsive LQR has been described and applied to the reconfiguration of Lorentz-augmented spacecraft formation. Since the optimality conditions require the value of the state at the impulse application time, a guess-and-check approach to determining the optimal times is proposed. For spacecraft applications, determination of the optimal times and calculation of the associated solution to the Riccati equation would need to occur on-ground-based computers and then communicated to the spacecraft. For a prescribed number of impulses over a control period, the optimal times for the impulses can be determined, however, the optimal number of impulses over a control interval remains an open problem.

It was shown that the use of such a controller is effective for Lorentz-augmented spacecraft formation reconfiguration.

Use of the Lorentz force as a means of actuation resulted in considerable reduction in the required thruster ΔV for a reconfiguration when compared with conventional impulsive reconfiguration strategies. The required specific charge magnitudes are at the limit of what is currently considered feasible.

REFERENCES

[1] M. A. Peck, "Prospects and challenges for Lorentz-augmented orbits," in *Proc. AIAA Guid., Navigat., Control Conf. Exhibit*, 2005, pp. 1–16.

[2] M. A. Peck, B. Streetman, C. M. Saaj, and V. Lappas, "Spacecraft formation flying using Lorentz forces," *J. Brit. Interplanetary Soc.*, vol. 60, pp. 263–267, Jul. 2007.

[3] H. Yamakawa, M. Bando, K. Yano, and S. Tsujii, "Spacecraft relative dynamics under the influence of geomagnetic Lorentz force," in *Proc. AIAA Guid., Navigat., Control Conf.*, 2010, pp. 1–13.

[4] G. E. Pollock, J. W. Gangestad, and J. M. Longuski, "Analytical solutions for the relative motion of spacecraft subject to Lorentz-force perturbations," *Acta Astron.*, vol. 68, nos. 1–2, pp. 204–217, 2011.

[5] S. Tsujii, M. Bando, and H. Yamakawa, "Spacecraft formation flying dynamics and control using the geomagnetic Lorentz force," *J. Guid., Control, Dyn.*, vol. 36, no. 1, pp. 136–148, 2013.

[6] L. Breger and J. P. How, "Gauss's variational equation-based dynamics and control for formation flying spacecraft," *J. Guid., Control, Dyn.*, vol. 30, no. 2, pp. 437–448, 2007.

[7] L. A. Sobiesiak and C. J. Damaren, "Hybrid periodic differential element control using the geomagnetic Lorentz force," in *Proc. AIAA/AAS Astrodyn. Specialist Conf.*, Minneapolis, MN, USA, Aug. 2012, pp. 1–12.

[8] L. A. Sobiesiak and C. J. Damaren, "Optimal hybrid control for Lorentz-augmented formation flying," in *Proc. AIAA Guid., Navigat., Control Conf.*, Boston, MA, USA, Aug. 2013, pp. 1–9.

[9] L. A. Sobiesiak and C. J. Damaren, "Optimal continuous/impulsive control for Lorentz-augmented spacecraft formations," *J. Guid., Control, Dyn.*, vol. 38, no. 1, pp. 151–157, Jan. 2015.

[10] P. Riedinger, F. Kratz, C. Iung, and C. Zanne, "Linear quadratic optimization for hybrid systems," in *Proc. 38th IEEE Conf. Decision Control*, Dec. 1999, pp. 3059–3064.

[11] J. Hu, H. Wang, X. Liu, and B. Liu, "Optimization problems for switched systems with impulsive control," *J. Control Theory Appl.*, vol. 3, no. 1, pp. 93–100, 2005.

[12] L. A. Sobiesiak and C. J. Damaren, "Linear quadratic optimal control for systems with continuous and impulsive inputs," in *Proc. IEEE 53rd Annu. Conf. Decision Control*, Los Angeles, CA, USA, Dec. 2014, pp. 5071–5076.

[13] L. A. Sobiesiak and C. J. Damaren, "Lorentz-augmented spacecraft formation reconfiguration," in *Proc. AIAA/AAS Astrodyn. Specialist Conf.*, San Diego, CA, USA, Aug. 2014, pp. 1–12.

[14] H. Schaub and K. T. Alfriend, "Impulsive feedback control to establish specific mean orbit elements of spacecraft formations," *J. Guid., Control, Dyn.*, vol. 24, no. 4, pp. 739–745, Jul./Aug. 2001.

[15] P. Sengupta, S. R. Vadali, and K. T. Alfriend, "Modeling and control of satellite formations in high eccentricity orbits," *J. Astron. Sci.*, vol. 52, nos. 1–2, pp. 149–168, Jan./Jun. 2004.

[16] S. S. Vaddi, K. A. Alfriend, S. R. Vadali, and P. Sengupta, "Formation establishment and reconfiguration using impulsive control," *J. Guid., Control, Dyn.*, vol. 28, no. 2, pp. 262–268, Mar./Apr. 2005.

[17] A. E. Bryson, Jr., and Y.-C. Ho, *Applied Optimal Control*. Waltham, MA, USA: Ginn, 1969.

[18] H. Kwakernaak and R. Sivan, *Linear Optimal Control Systems*. New York, NY, USA: Wiley, 1972.

[19] H. Geering, "Continuous-time optimal control theory for cost functionals including discrete state penalty terms," *IEEE Trans. Autom. Control*, vol. 21, no. 6, pp. 866–869, Dec. 1976.

[20] H. Schaub, S. R. Vadali, J. L. Junkins, and K. T. Alfriend, "Spacecraft formation flying control using mean orbit elements," *J. Astron. Sci.*, vol. 48, no. 1, pp. 69–87, Jan./Mar. 2000.

[21] H. Schaub and J. L. Junkins, *Analytical Mechanics of Space Systems*, J. A. Schetz, Ed. Washington, DC, USA: AIAA, 2003.

[22] R. H. Battin, *An Introduction to the Mathematics and Methods of Astrodynamics*, J. Przemieniecki, Ed. Washington, DC, USA: AIAA, 1999.

[23] H. Schaub and K. T. Alfriend, "Hybrid Cartesian and orbit element feedback law for formation flying spacecraft," *J. Guid., Control, Dyn.*, vol. 25, no. 2, pp. 387–393, 2002.

[24] C. C. Finlay *et al.*, "International geomagnetic reference field: The eleventh generation," *Geophys. J. Int.*, vol. 183, no. 3, pp. 1216–1230, 2010.

[25] C. Saaj, V. Lappas, D. Richie, M. A. Peck, B. Streetman, and H. Schaub, "Electrostatic forces for satellite navigation and reconfiguration," Dept. Ariadna Final, Eur. Space Agency, Paris, France, Tech. Rep. 05-4107b, 2006.

[26] B. Streetman and M. A. Peck, "General bang–bang control method for Lorentz augmented orbits," *J. Spacecraft Rockets*, vol. 47, no. 3, pp. 484–492, 2010.

Ludwik A. Sobiesiak received the B.A.Sc. degree in mechatronics engineering from the University of Waterloo, Waterloo, ON, Canada, in 2009, and the Ph.D. degree in aerospace engineering from the University of Toronto, Toronto, ON, Canada, in 2014.

He is currently a Flight Dynamics Analyst with Telesat, Ottawa, ON, Canada. His current research interests include spacecraft formation control and relative state estimation, and autonomous control and localization strategies for unmanned aerial vehicles.

Christopher J. Damaren was born in Toronto, ON, Canada, in 1962. He received the B.A.Sc. degree in engineering science (aerospace option) from the University of Toronto, Toronto, in 1985, and the M.A.Sc. and Ph.D. degrees in aerospace engineering from the University of Toronto Institute for Aerospace Studies (UTIAS), North York, ON, Canada, in 1987 and 1990, respectively.

He was an Assistant Professor with the Department of Engineering, Royal Roads Military College, Victoria, BC, Canada, from 1990 to 1995. From 1995 to 1999, he was a Senior Lecturer with the Department of Mechanical Engineering, University of Canterbury, Christchurch, New Zealand. Since 1999, he has been with UTIAS and is currently a Professor. His current research interests include dynamics and control of space systems.

Prof. Damaren is a Fellow of the Canadian Aeronautics and Space Institute and an Associate Fellow of the American Institute of Aeronautics and Astronautics.